Rarefaction waves in van der Waals fluids with an arbitrary number of degrees of freedom

Albert Yuen[*]
Department of Nuclear Engineering, University of California, Berkeley, California 94720, USA
and Lawrence Berkeley National Laboratory, Berkeley, California 94720, USA

John J. Barnard[†]
Lawrence Livermore National Laboratory, Livermore, California 94550, USA
(Received 8 March 2015; published 30 September 2015)

The isentropic expansion of an instantaneously and homogeneously heated foil is calculated using a 1D fluid model. The initial temperature and density are assumed to be in the vicinity of the critical temperature and solid density, respectively. The fluid is assumed to satisfy the van der Waals equation of state with an arbitrary number of degrees of freedom. Self-similar Riemann solutions are found. With a larger number of degrees of freedom f, depending on the initial dimensionless entropy $\tilde{s}_0$, a richer family of foil expansion behaviors have been found. We calculate the domain in parameter space where these behaviors occur. In total, eight types of rarefaction waves are found and described.

DOI: 10.1103/PhysRevE.92.033019 PACS number(s): 47.35.−i, 64.10.+h, 51.30.+i, 64.60.−i

I. INTRODUCTION

Warm dense matter (WDM) conditions are reached when the density is approximately in the range of 0.1 to 10 times the solid density and the temperature approximately reaches 0.01 to 10 eV, although some authors extend the WDM regime to temperatures up to 50 eV [1,2]. WDM conditions occur naturally and artificially, e.g., in the core of gaseous planets [3], during the heating of a metal by a laser [3–5] or an ion beam [5–8], or during the early stages of an inertial confined fusion implosion [9].

This paper focuses on the hydrodynamical expansion and transition of a material from a high temperature liquid or solid state into a vapor state, which, for some materials, is in the WDM regime. Emphasis is made on the conditions around the critical point, above which there is no distinction between the liquid and vapor phases. For many materials such as refractory metals [10], the full vapor-liquid phase boundary as a function of density and temperature is poorly known.

Riemann [11] proved that, for any equation of state (EOS) and if the motion is 1D, the flow of an instantaneously heated semiinfinite foil is self-similar, and analytically derived the dynamics of the flow for the case of an ideal gas (see also Refs. [12] and [13]). The present paper uses Riemann's solution for the specific case where the matter behaves as a van der Waals (VDW) fluid.

Under certain conditions, the solution displays plateaus of constant density during the phase transition from a single-phase to the two-phase regime. The plateaus may have observational consequences. For example, optical fringes in reflected laser light have been observed in short-pulse laser experiments on Si surfaces [14]. The optical fringes were later interpreted as density plateaus of the flow [6,15–17]. Density plateaus of the flow have also been observed semianalytically and numerically for particular choices of parameters of VDW fluids in expansion [18]. By describing the expanding matter as a polytropic fluid (i.e., following the relation $p \propto \rho^{(n+1)/n}$, where p, ρ, n are, respectively, the fluid pressure, mass density, and the polytropic index), it was also observed analytically and numerically that the flow of the expanding matter consists of two domains: a thin liquid shell moving with constant velocity and a thick low-density layer of material in a two-phase state [19]. The solutions for two different polytropes were subsequently patched together and reproduced qualitatively the features observed using a more detailed yet complex equation of state for aluminum.

Other work has shown that a single measurement of the density profile (as a function of distance) for an expanding 1D material can be used to infer the pressure as a function of density [20]. Previous work on hydrodynamic waves in generalized VDW fluids in the vicinity of the two-phase regime, but still above the critical point, showed the possible presence of rarefaction shockwaves, particularly for foils of finite thickness [12,21–23].

The present paper treats simple-wave-based solutions, i.e., before the rarefaction waves from both sides of a given thin foil meet. The more complex problem where these two rarefaction waves meet at the center has been treated analytically for an ideal gas [13]. Here, a 1D fluid model with a generalized VDW EOS is employed to find the types of rarefaction waves and their inherent features in the dynamics of the foil expansion, both semianalytically (by numerically integrating a system of ODEs) and numerically using the 1D planar Lagrangian hydrodynamic code DISH [24]. In this paper, we categorize the possible types of rarefaction waves in generalized VDW fluids.

II. GEOMETRY AND METHOD

The initial foil is modeled by a 1D semiinfinite slab of material that initially extends from $z = -\infty$ to $z = 0$, and from $-\infty$ to $+\infty$ in the x and y directions. In spite of being 1D planar, the model is nevertheless a good approximation for higher-dimensional geometries at early times, since the out-flowing material would extend to distances much smaller than the radius of the heating beam. For later times, 2D and 3D solutions of the hydrodynamics equations introduce new

[*]albert.yuen@berkeley.edu
[†]jjbarnard@lbl.gov

characteristic length scales, e.g., curvature radius, making a self-similar solution impossible.

The foil at initial density ρ_0 is assumed to have undergone uniform and instantaneous heating to temperature T_0. This is a valid assumption when the heating time is much shorter than the hydrodynamic time—the time for the rarefaction wave to reach the center of the foil—and when the deposition is volumetric, as with x-ray or ion beam heating.

A fluid description employing the VDW EOS is used to describe the dynamics of the heated target. The VDW EOS is a "cubic" EOS (i.e., one in which the density expressed as a function of P and T is the solution of a cubic equation in ρ), chosen in this paper for its mathematical simplicity and its two-phase behavior. The VDW picture for monoatomic fluids assumes (i) a hard-sphere representation of atoms in a fluid, (ii) a meaningful separation of potential into a strong short-ranged repulsive part and a weaker long-ranged attractive part, (iii) that the weaker long-ranged attractive forces can be modeled as a mean field, (iv) and that intermolecular hydrogen bonds, directional intermolecular covalent bonds, and ionic forces are negligible. In this paper, we employ a generalized version (see, e.g., Ref. [21]) that includes internal degrees of freedom and enables richer physics of internal modes, e.g., molecular rotations and vibrations can be included. The simplifications adopted in items (i) through (iv) above restrict the applicability of the VDW EOS and may hinder quantitative investigations of rarefaction waves using the VDW EOS. However, the VDW picture has been successfully applied to interpret a wide range of condensed matter properties [25] and can be improved in order to quantitatively investigate a broader set of fluids for design purposes [26]. In this paper, our intent is to give a concrete example of the variety of behaviors that can occur for an equation of state that exhibits a liquid-vapor phase change. The simplicity of the EOS allows us to identify the boundaries in a dimensionless two-parameter space for the eight classes of rarefaction waves identified in this study. It is often useful to compare experimental data with known (but idealized) solutions to the fluid equations. We also believe these similarity solutions could be useful in benchmarking more complicated hydrodynamic codes.

The Maxwell construction is also employed in order to avoid the microinstabilities that occur during a phase transition. However, because it is an equilibrium theory, the Maxwell construction cannot model droplets and bubbles created in the two-phase regime. The numerically challenging problem of resolving droplets and bubbles in a simulation [27] could yield a more accurate description of the rarefaction waves.

III. HYDRODYNAMICS OF THE VAN DER WAALS FLUID

A. Hydrodynamics

The continuity and momentum equations for a neutral and nonviscous fluid in the absence of a mass source or sink for the 1D Cartesian Eulerian fluid system [11–13] are

$$\begin{aligned} \frac{\partial \rho}{\partial t} + \frac{\partial \rho v}{\partial z} &= 0, \\ \frac{\partial v}{\partial t} + v\frac{\partial v}{\partial z} &= -\frac{1}{\rho}\frac{\partial p}{\partial z}. \end{aligned} \tag{1}$$

Here, ρ, p, and v are, respectively, the fluid mass density, pressure, and velocity at time t and axial coordinate z.

Equation (1) decouples by employing $P = v + I$ and $M = v - I$ with $I(\rho) = \int_{\rho_0}^{\rho} \frac{c_s(\rho')}{\rho'}\, d\rho'$ and c_s the sound speed defined as ${c_s}^2(\rho) = \partial p/\partial\rho|_s$. ρ_0 is the density of the uniformly heated fluid at the initial time $t = 0$. The subscript s means that the derivative is taken at constant entropy. The use of the self-similar variable $\xi = z/t$ eliminates an independent variable, and writing $'$ as the total derivative with respect to ξ, Eq. (1) simplifies to

$$\begin{aligned} (v + c_s - \xi)P'(\xi) &= 0, \\ (v - c_s - \xi)M'(\xi) &= 0, \end{aligned} \tag{2}$$

which yields

$$(v - c_s - \xi) = 0 \quad \text{and} \quad P'(\xi) = 0, \tag{3a}$$

$$\text{or } (v + c_s - \xi) = 0 \quad \text{and} \quad M'(\xi) = 0. \tag{3b}$$

For a typical EOS ($\partial p/\partial V^2|_s > 0$), the asymptotic solutions of the system set conditions on the sound speed and the fluid velocity. In the dense fluid, i.e., for $\xi \ll 0$, the sound speed must be nonzero and the fluid velocity equal to zero. In the vacuum side, i.e., for $\xi \gg 0$, the sound speed must tend to zero and the fluid velocity must be positive. Equivalently,

$$\begin{aligned} &\text{for } \xi \ll 0,\ c_s > 0 \quad \text{and} \quad v \to 0, \\ &\text{and for } \xi \gg 0,\ c_s \to 0 \quad \text{and} \quad v > 0. \end{aligned} \tag{4}$$

Because Eq. (3b) does not fulfill the asymptotic conditions of Eq. (4), Eq. (3a) is the valid solution and sets the hydrodynamics equation,

$$\xi(\rho) = -I(\rho) - c_s(\rho). \tag{5}$$

$c_s(\rho)$ depends on the thermodynamical properties of the fluid expansion, henceforth modeled by the VDW EOS.

B. Equation of state: The generalized van der Waals model

The VDW EOS is described by the following equations:

$$p = \frac{\rho kT}{Am_{\text{amu}}(1 - b\rho)} - a\rho^2, \tag{6a}$$

$$s = \frac{k}{Am_{\text{amu}}} \ln\left(Am_{\text{amu}} \frac{1 - b\rho}{\rho} \frac{\lambda_0^{f-3}}{\lambda^f} \right), \tag{6b}$$

$$c_s^2 = \left.\frac{\partial p}{\partial \rho}\right|_s = \frac{f+2}{f}\frac{kT}{Am_{\text{amu}}}\frac{1}{(1 - b\rho)^2} - 2a\rho, \tag{6c}$$

$$\epsilon = \frac{f}{2}\frac{kT}{Am_{\text{amu}}} - a\rho. \tag{6d}$$

Here, p, ρ, T, s, c_s, and ϵ are, respectively, the pressure, mass density, temperature, entropy, sound speed, and the energy density of the fluid. A is the mass number of the atomic species of the fluid, k is the Boltzmann constant, and m_{amu} is the atomic mass unit. $\lambda = h/(2\pi Am_{\text{amu}}kT)^{1/2}$ is the de Broglie wavelength. h is the Planck constant. λ_0 is an arbitrary normalization constant that has no effect on the dynamics and will not appear in the subsequent treatment of the rarefaction waves. a and b are the VDW constants of the fluid whose derivations can be found in the literature [28] and whose

experimental values can be found in reference tables [29] for a number of gases and compounds, but, for many materials that have high critical temperatures, the constants have not been measured or yield large measurement uncertainties [10]. In Eq. (6) and throughout this paper, the VDW EOS has been generalized to arbitrary numbers of degrees of freedom $f \geqslant 3$ in order to account for more complex material compounds. The standard VDW EOS for monatomic molecules has a number of degrees of freedom $f = 3$. In Eq. (6a), the first term in the right-hand side models the strong short-ranged repulsive atomic forces while the second term models the long-ranged attractive forces.

The critical pressure p_c, density ρ_c, and temperature T_c are defined at the inflection point $\partial p/\partial\rho|_T = \partial^2 p/\partial\rho^2|_T = 0$ and yield

$$\rho_c = \frac{1}{3b}, \quad p_c = \frac{1}{27}\frac{a}{b^2}, \quad \text{and} \quad \frac{kT_c}{Am_{\text{amu}}} = \frac{8}{27}\frac{a}{b}. \tag{7}$$

Furthermore, a characteristic sound speed $c_{s,0}^2 = p_c/\rho_c$ and a characteristic energy density $\epsilon_c = \epsilon(\rho_c, T_c) = (4f - 9)/27 \times a/b$ are defined based on the critical parameters. Note $c_{s,0}^2$ is not the sound speed at the critical point, rather a characteristic speed that we chose to simplify the equations. The sound speed at the critical point is $2\sqrt{3/f}\, c_{s,0}$.

For generality, dimensionless quantities are henceforth employed by scaling all dimensional quantities with the critical or characteristic parameters above-mentioned. In what follows, tilded quantities are the dimensionless counterparts of dimensional quantities such that $\tilde\rho = \rho/\rho_c$, $\tilde p = p/p_c$, $\tilde T = T/T_c$, $\tilde c_s(\tilde\rho) = c_s(\rho)/c_{s,0}$, and $\tilde\epsilon = \epsilon/\epsilon_c$.

From Eqs. (6) and (7), the dimensionless VDW equations yield

$$\tilde p = 8\frac{\tilde\rho\tilde T}{3-\tilde\rho} - 3\tilde\rho^2, \tag{8a}$$

$$\tilde s = \frac{s - s_c}{k/(Am_{\text{amu}})} = \ln\left(\frac{3-\tilde\rho}{2\tilde\rho}\tilde T^{f/2}\right), \tag{8b}$$

$$\tilde c_s^2 = \left.\frac{\partial\tilde p}{\partial\tilde\rho}\right|_{\tilde s} = \frac{f+2}{f}\frac{24\tilde T}{(3-\tilde\rho)^2} - 6\tilde\rho, \tag{8c}$$

$$\tilde\epsilon = \frac{4f}{4f-9}\tilde T - \frac{9}{4f-9}\tilde\rho. \tag{8d}$$

Here, $s_c = s(\rho_c, T_c)$. There exists a regime of instability where $\partial\tilde p/\partial\tilde\rho|_{\tilde T} < 0$ for the isotherms $\tilde T < 1$ since the density increases for a decreasing pressure, which is unphysical for a fluid in equilibrium. Consequently, the Maxwell construction [30] is employed to represent an equilibrium state in this unstable zone: the fluid is modeled as a mixture of a liquid phase of density $\tilde\rho_l$ and pressure $\tilde p_l$ at mass fraction x_l and a gaseous phase of density $\tilde\rho_g$ and pressure $\tilde p_g$ at mass fraction x_g. The Maxwell construction sets $\tilde\rho_l$, $\tilde\rho_g$, $\tilde p_l$, and $\tilde p_g$ by assuming equal pressure $\tilde p$ and chemical potential $\tilde\mu$ between the two phases; i.e., $\tilde p_l(\tilde T) = \tilde p_g(\tilde T)$ and $\tilde\mu_l(\tilde T) = \tilde\mu_g(\tilde T)$. The latter condition is equivalent to $\int_{\tilde V_l}^{\tilde V_g}(\tilde p - \tilde p_g)\, d\tilde V = 0$. Here $\tilde V = 1/\tilde\rho$ is the dimensionless specific volume.

The liquid and gas mass fraction x_l and x_g is defined by

$$\begin{aligned} x_l(\tilde\rho,\tilde T) &= \frac{\tilde\rho_l(\tilde T)}{\tilde\rho}\frac{\tilde\rho - \tilde\rho_g(\tilde T)}{\tilde\rho_l(\tilde T) - \tilde\rho_g(\tilde T)}, \\ x_g(\tilde\rho,\tilde T) &= \frac{\tilde\rho_g(\tilde T)}{\tilde\rho}\frac{\tilde\rho - \tilde\rho_l(\tilde T)}{\tilde\rho_g(\tilde T) - \tilde\rho_l(\tilde T)}. \end{aligned} \tag{9}$$

The emphasis in this paper is on the isentropic evolution of the VDW fluid, i.e., $\tilde s(\tilde\rho,\tilde T) = \tilde s_0$ is constant where $\tilde s_0$ is the initial dimensionless entropy of the fluid. This hypothesis eliminates one of the two independent parameters in Eq. (9) and yields

$$\begin{aligned} x_l(\tilde T) &= \ln\left(\frac{3-\tilde\rho_0}{3-\tilde\rho_g}\frac{\tilde\rho_g}{\tilde\rho_0}\left(\frac{\tilde T_0}{\tilde T_g}\right)^{f/2}\right)\Big/\ln\left(\frac{3-\tilde\rho_l}{3-\tilde\rho_g}\frac{\tilde\rho_g}{\tilde\rho_l}\right), \\ x_g(\tilde T) &= \ln\left(\frac{3-\tilde\rho_0}{3-\tilde\rho_l}\frac{\tilde\rho_l}{\tilde\rho_0}\left(\frac{\tilde T_0}{\tilde T_l}\right)^{f/2}\right)\Big/\ln\left(\frac{3-\tilde\rho_g}{3-\tilde\rho_l}\frac{\tilde\rho_l}{\tilde\rho_g}\right). \end{aligned} \tag{10}$$

The density in the two-phase regime may be expressed as a function of temperature only:

$$\tilde\rho(\tilde T) = \frac{\tilde\rho_l(\tilde T)\tilde\rho_g(\tilde T)}{x_g(\tilde T)\tilde\rho_l(\tilde T) + x_l(\tilde T)\tilde\rho_g(\tilde T)}. \tag{11}$$

To complete the calculation of the self-similar evolution, we need to calculate the sound speed in the two-phase regime. Since the pressure may be written as a function of the temperature only $\tilde p(\tilde T) = \tilde p(\tilde\rho_l(\tilde T),\tilde T) = \tilde p(\tilde\rho_g(\tilde T),\tilde T)$, the sound speed may be calculated, $\tilde c_s^2 = \frac{\partial\tilde p(\tilde s,\tilde\rho)}{\partial\tilde\rho}|_{\tilde s} = \frac{d\tilde p(\tilde T)/d\tilde T}{d\tilde\rho(\tilde T)/d\tilde T}$, so that $\tilde I(\tilde\rho)$ is the sum of the contribution before entering the two-phase regime plus the contribution in the two-phase regime: $\tilde I(\tilde\rho) = \int_{\tilde\rho_0}^{\tilde\rho_b}\frac{\tilde c_s(\tilde\rho)}{\tilde\rho}d\tilde\rho + \int_{\tilde\rho_b(\tilde T_b)}^{\tilde\rho(\tilde T)}\frac{\tilde c_s(\tilde\rho)}{\tilde\rho}\frac{d\tilde\rho}{d\tilde T}d\tilde T$.

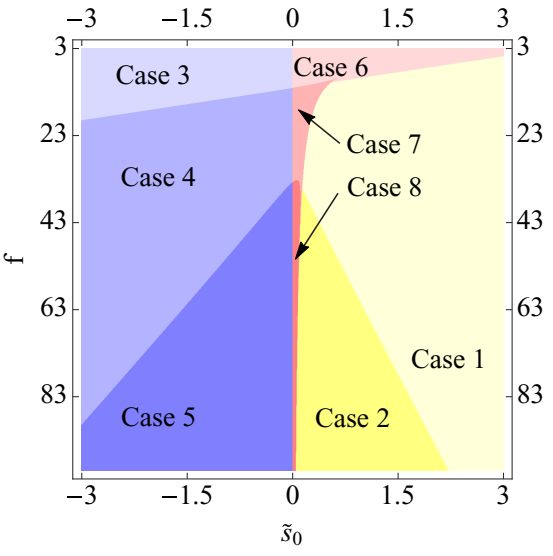

FIG. 1. (Color online) Diagram determining which type of rarefaction waves to encounter depending on initial entropy $\tilde s_0$ and number of degrees of freedom f.

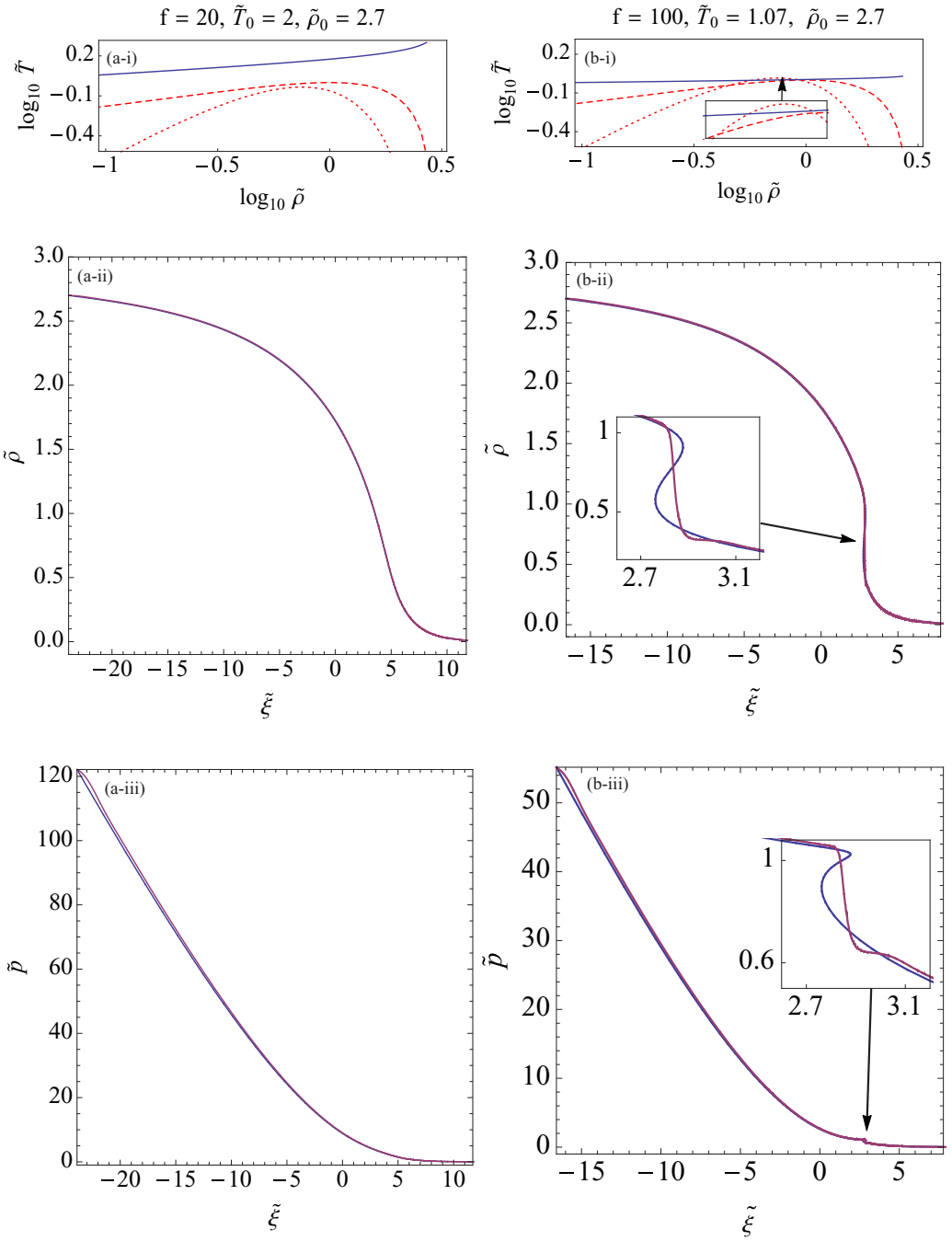

FIG. 2. (Color online) The rarefaction waves of (a) case 1 and (b) case 2. Each of the subfigures contains three plots. In the (i) subfigures of each cases are represented in full blue line the isentropic trajectory of the rarefaction wave, in dashed red line the Maxwell-constructed binodal between single- and two-phase regime, and in dotted line the unstable boundary in the single-phase regime. In the (ii) and (iii) subfigures of each cases are represented in blue line the semianalytical solution, and the purple line is the numerical solution of the density and pressure profiles. Zones of interest of the rarefaction waves are zoomed.

It can be shown [12] that a shockwave is possible when $d^2\tilde{\rho}/d\tilde{V}^2|_{\tilde{s}} < 0$ and their existence has been numerically predicted for a foil of finite thickness modeled as a single phase VDW fluid (subsequently referred to as case 1 and case 2 in Fig. 2) in the complex wave regime [21], i.e., when the rarefaction waves from the ends of the foil meet.

Eight types of rarefaction waves that depend exclusively on the initial entropy and the number of degrees of freedom, as shown in Fig. 1, are found from the isentropic trajectory of the VDW fluid in the $(\tilde{\rho}, \tilde{T})$ diagram and are plotted as a blue full line in the eight upper subplots of the $(\tilde{\rho}, \tilde{T})$ diagrams in Figs. 2, 3, and 4. Also depicted in the upper subplots of Figs. 2, 3, and 4 are the Maxwell-constructed binodal between the single-phase regime and two-phase regime in red dashed line and the shockwave boundary in red dotted line. Note that even though the shockwave boundary in red dotted line is

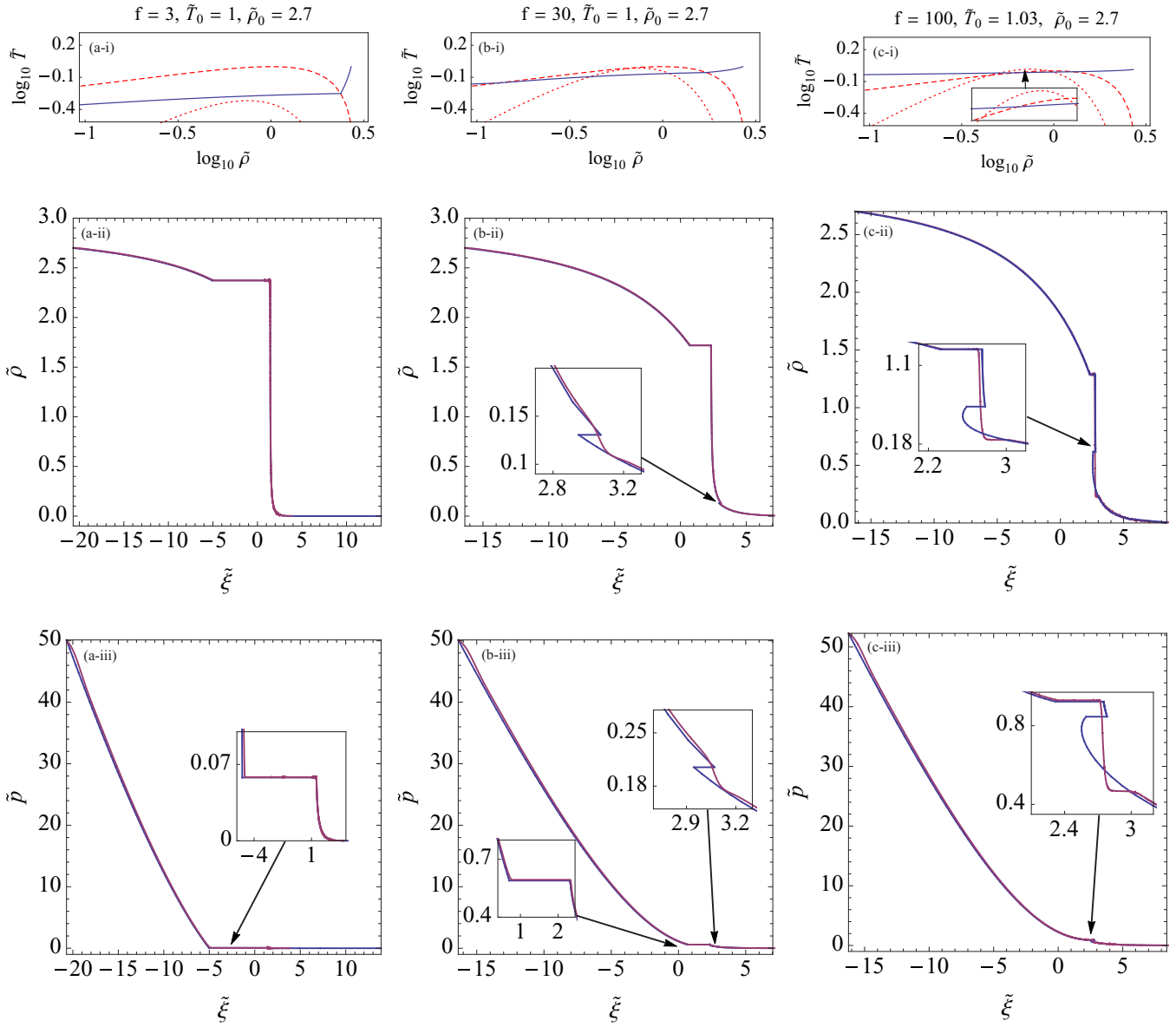

FIG. 3. (Color online) The rarefaction waves of (a) case 3, (b) case 4, and (c) case 5 are displayed. See annotations of Fig. 2 for details.

valid only in the single-phase regime, it has been included in all the diagrams even when it is not valid in order to see the proximity of the shock regime to the single-phase regime. For $f > 34$, shockwaves can be observed for some isentropes [23] since part of the shockwave boundary is above the Maxwell-constructed binodal.

As expected, these isentropic trajectories in the $(\tilde{\rho}, \tilde{T})$ diagram yield different shapes of density and pressure profiles in the next section.

C. Dimensionless solutions

The hydrodynamic Eq. (5) is scaled by $c_{s,0}$ and yields

$$\tilde{\xi}(\tilde{\rho}) = -\tilde{I}(\tilde{\rho}) - \tilde{c}_s(\tilde{\rho}), \tag{12}$$

which completes the set of dimensionless equations. Here, $\tilde{\xi}(\tilde{\rho}) = \xi(\rho)/c_{s,0}$, $\tilde{I}(\tilde{\rho}) = I(\rho)/c_{s,0}$, and $\tilde{c}_s(\tilde{\rho}) = c_s(\rho)/c_{s,0}$.

This analysis is applicable to any VDW fluid as the solutions can be scaled back to dimensional quantities using the appropriate A, a, and b that characterize a given chemical element.

In the following, we denote the variables with subscript "b" their values at binodal. While $\partial\tilde{p}/\partial\tilde{\rho}|_{\tilde{T}}$ no longer reaches negative values due to the Maxwell construction, it is no longer a smooth function of $\tilde{\rho}$ at $\tilde{\rho} = \tilde{\rho}_b$ as $\partial\tilde{p}/\partial\tilde{\rho}|_{\tilde{T}}(\tilde{\rho}_b^+) \neq \partial\tilde{p}/\partial\tilde{\rho}|_{\tilde{T}}(\tilde{\rho}_b^-)$, which leads to the discontinuity of the sound speed at $\tilde{\rho} = \tilde{\rho}_b$. From Eq. (12), a discontinuity in $\tilde{\xi}$ is therefore expected each time an isentropic trajectory crosses the Maxwell-constructed binodal in the $(\tilde{p}, \tilde{\rho})$ diagram.

This set of dimensionless equations is semianalytically solved using Mathematica [31] and compared against the 1D planar Lagrangian hydrodynamic code DISH [24].

The density $\tilde{\rho}$ and pressure $\tilde{p}$ profiles as a function of the self-similar variable $\tilde{\xi}$ of each of the eight types of rarefaction waves under investigation are represented in the central and lower parts of Figs. 2, 3, and 4. As the density

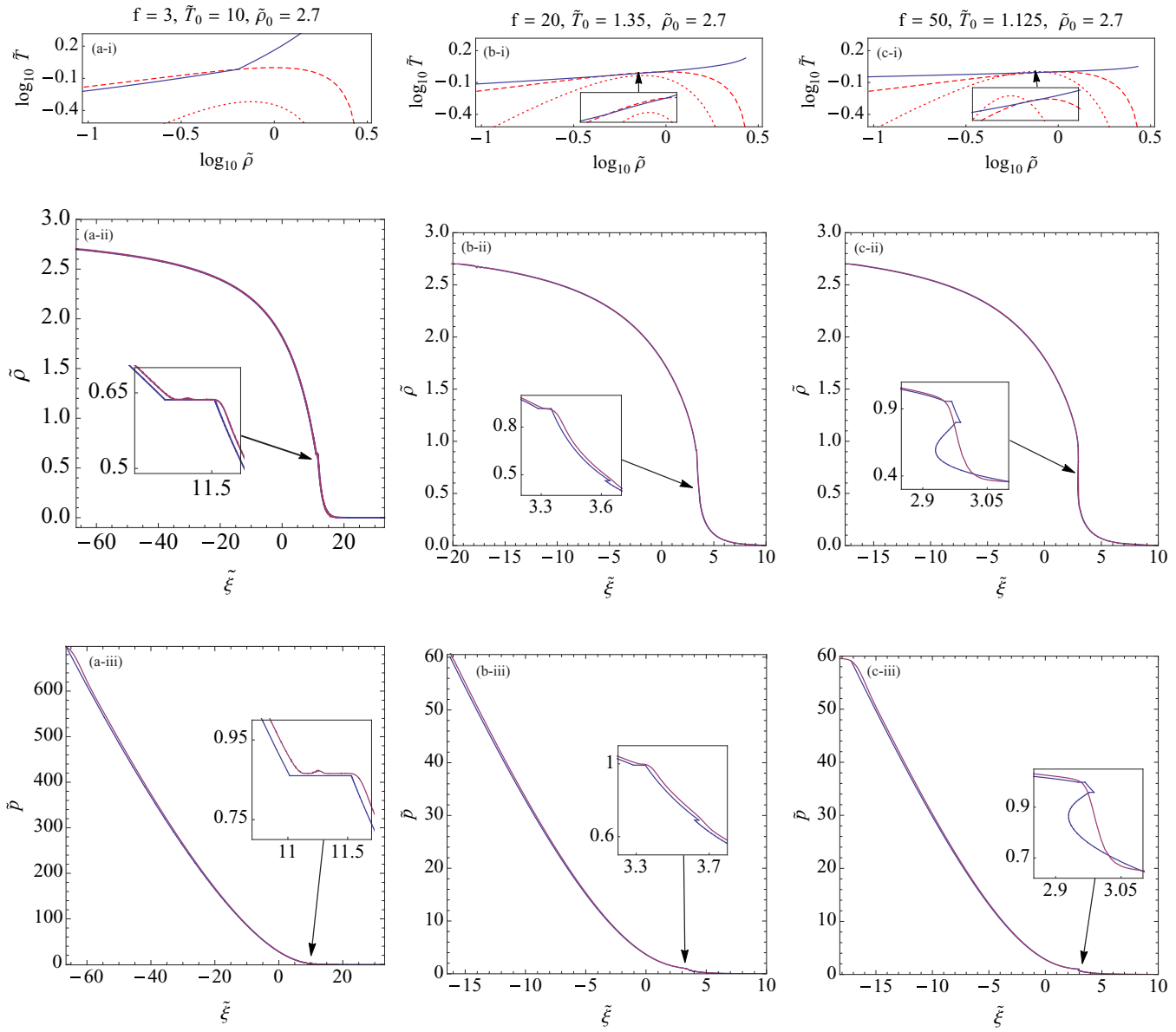

FIG. 4. (Color online) The rarefaction waves of (a) case 6, (b) case 7, and (c) case 8 are displayed. See annotations of Fig. 2 for details.

and pressure profiles computed numerically by the DISH code also displayed a self-similar expansion, they are also plotted in dimensionless variables as a function of the self-similar variable. In each of those cases, the numerical simulations showed that the entropy is conserved.

In cases 1, 3, and 6 the semianalytic similarity solution and the hydrodynamic code DISH agree well. The plateau region in density, temperature, pressure, and velocity that occurs in the transition to the two-phase regime (in cases 3 and 6) is faithfully reproduced in DISH as well as in the semianalytic similarity solution.

In cases 2, 4, 5, 7, and 8, the fluid follows a trajectory such that $\partial^2\tilde{p}/\partial\tilde{V}^2|_{\tilde{s}}$ is less than zero for a part of the fluid's trajectory in the $(\tilde{\rho},\tilde{T})$ diagram (where $\tilde{V}\equiv 1/\tilde{\rho}$). As indicated in Refs. [12,21], this implies an unstable region where shocks may form. A simple integration of the semianalytic solution yields a double valued (unphysical) density distribution (see Figs. 2, 3, and 4). The DISH code yields a sharp density gradient in this unstable region (shown in purple), although it is well resolved (see Fig. 5) and does not have a discontinuity in the pressure and so is technically not a shock. The asymptotic density, temperature, and pressure before and after the unstable region (where $\partial^2\tilde{p}/\partial\tilde{V}^2|_{\tilde{s}}<0$) are nearly identical in the semianalytic solution and in DISH. The solution in the unstable region indicates a strong density and pressure gradient, followed by a more conventional rarefaction wave.

Case 1: $f=20$, $\tilde{T}_0=2$, $\tilde{\rho}_0=2.7$.
The fluid stays in one phase continuously varying from high-density fluid to a gas. The rarefaction wave does not display any plateau or unstable features. There is a good agreement between the semianalytical solution and the numerical solution (DISH).

Case 2: $f=100$, $\tilde{T}_0=1.07$, $\tilde{\rho}_0=2.7$.
The fluid stays in one phase continuously varying from high-density fluid to a gas. Because $f>34$, as previously mentioned, the shockwave boundary is above the Maxwell-

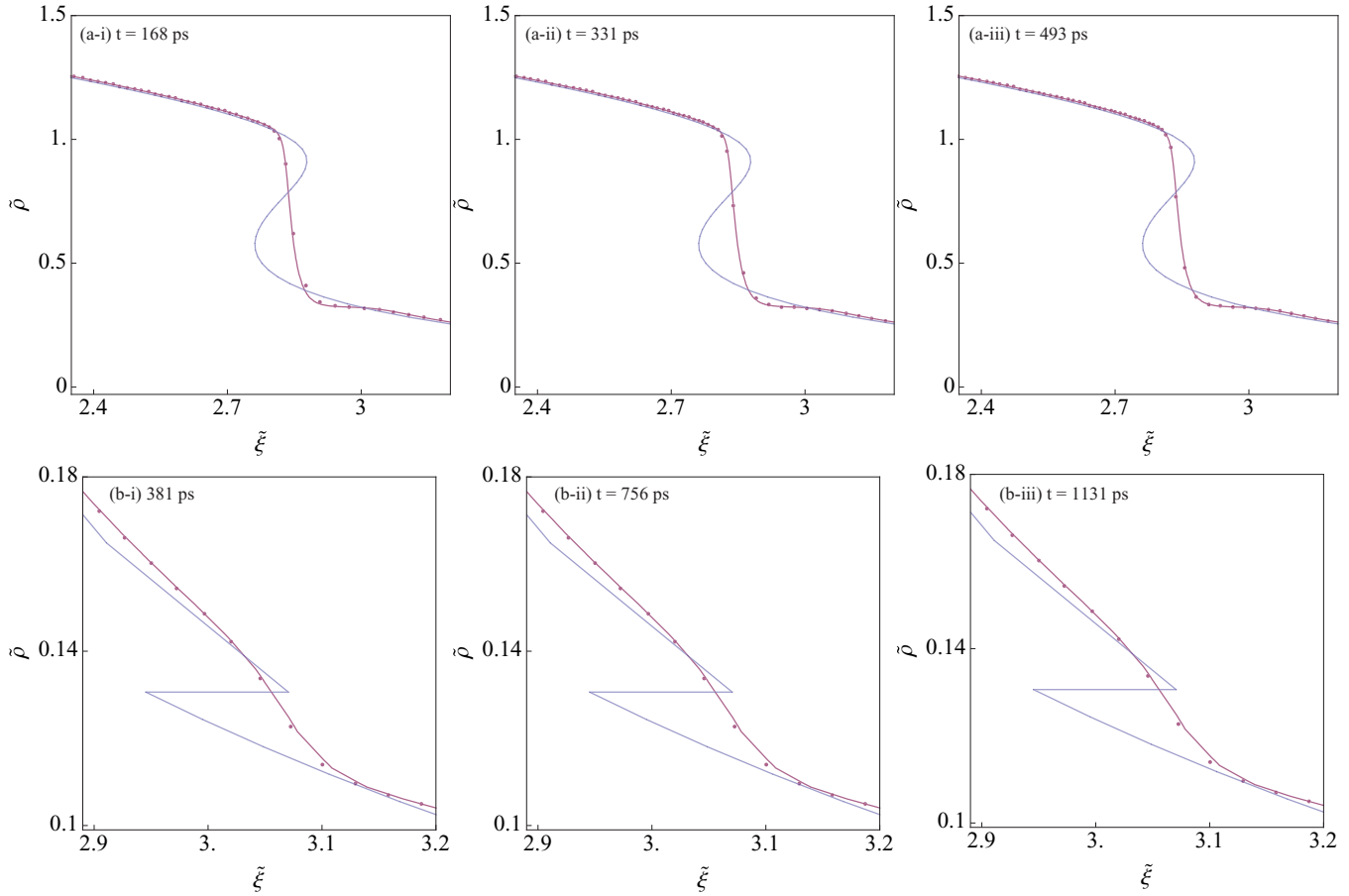

FIG. 5. (Color online) The numerically computed temporal evolution of the density profiles (in purple lines) shows that the kinks of the semianalytical solutions (in blue lines) are well resolved, and the evolution remains self-similar. The purple line is the interpolation of the numerical solution over time ranging from t_1 to t_3. The purple dots represent the numerical solution at a given time t_1, t_2, and t_3. (a) Case 2 ($\tilde{\rho}_0 = 2.7$, $\tilde{T}_0 = 1.07$, $f = 100$). (b) Case 4 ($\tilde{\rho}_0 = 2.7$, $\tilde{T}_0 = 1$, $f = 30$). The subfigures (i), (ii), and (iii) represent different snapshots at different times, as denoted on the figures.

constructed binodal in the $(\tilde{p}, \tilde{\rho})$ diagram. The studied case crosses the shock boundary. A self-similar pressure gradient forms in the numerical simulation and nonphysical "z"-shaped density and pressure profiles occur in the semianalytical solution. The semianalytical and numerical models not do agree, as the same analytical model evidently does not model well the unstable region, well-resolved numerically as shown in Fig. 5.

Case 3: $f = 3$, $\tilde{T}_0 = 1$, $\tilde{\rho}_0 = 2.7$.
The fluid starts as a single-phase fluid, enters the two-phase regime as a liquid, and stays as a two-phase fluid. A single-density plateau whose length is a function of $\tilde{s}$ and f is observed. There is a good agreement between the semianalytical solution and the numerical solution.

Case 4: $f = 30$, $\tilde{T}_0 = 1$, $\tilde{\rho}_0 = 2.7$.
The fluid starts as a single-phase fluid, enters the two-phase regime as a liquid, and leaves the two-phase regime to revert to a single phase that is gaseous. The rarefaction wave yields one plateau and a kink. The kink that can be observed in the semianalytical solution is simulated as a steep self-similar profile in the well-resolved numerical simulations (see Fig. 5), not modeled in our analytical model.

Case 5: $f = 100$, $\tilde{T}_0 = 1.03$, $\tilde{\rho}_0 = 2.7$.
The fluid starts as a single-phase fluid, becomes a liquid, enters the two-phase regime, and then quickly leaves the two-phase regime to revert as a single gaseous phase in the shockwave regime. This case is similar to case 4 with features from case 2.

Case 6: $f = 3$, $\tilde{T}_0 = 10$, $\tilde{\rho}_0 = 2.7$.
The fluid starts as a single-phase fluid, enters the two-phase regime as a gas, and stays as a two-phase fluid. Similar to case 3, a single-density plateau whose length is a function of $\tilde{s}$ and f is observed. The length of the plateau is smaller than case 3 and the shape of the rarefaction wave is more similar to case 1. There is a good agreement between the semianalytical solution and the numerical solution. Here, the bump in the purple numerical profiles is due to numerical artifacts as the steep gradient is difficult to resolve in the our hydrodynamic code. This case has similar features to case 3.

Case 7: $f = 20$, $\tilde{T}_0 = 1.35$, $\tilde{\rho}_0 = 2.7$.
The fluid starts as a single-phase fluid, enters the two-phase regime as a gas, and quickly leaves the two-phase regime to revert to a single gaseous phase. This case has similar features to case 4.

Case 8: $f = 50$, $\tilde{T}_0 = 1.125$, $\tilde{\rho}_0 = 2.7$.
The fluid starts as a single-phase fluid, becomes a gas, enters the two-phase regime, and then quickly leaves the two-phase regime to revert as a single gaseous phase in the shockwave regime. This case has similar features to case 5.

IV. DISCUSSIONS

The 1D planar isentropic hydrodynamic model of a generalized van der Waals fluid homogeneously and instantaneously heated to temperatures of order the critical point predicts the presence of eight types of rarefaction waves depending on the number of degrees of freedom f, the initial density ρ_0, and temperature T_0 in the simple-wave regime.

Our work shows that for certain values of f and $\tilde{s}_0$ in the simple-wave regime, the fluid can go through a region of instability ($\partial^2\tilde{p}/\partial\tilde{V}^2|_{\tilde{s}} < 0$), in which a strong pressure gradient (possibly a shock) forms. This is not in disagreement with Ref. [21], which found that shocks formed in the nonsimple wave regime, after the rarefaction waves collided in the middle of the foil. Interestingly, the numerical solutions in the unstable regime appear to be self-similar as seen from overlaying density and pressure profiles from different times. Nevertheless, the numerical solutions do not show the formation of a shock wave. We have not resolved this discrepancy and can only conclude that a steep density gradient (if not a shock) forms in the unstable regime.

This work should be useful in interpreting and categorizing the types of behavior observed when experiments are carried out that produce warm dense matter conditions by volumetrically heating thin foils and using the subsequent dynamic behavior to infer properties of the matter.

ACKNOWLEDGMENTS

The authors are pleased to acknowledge numerous valuable discussions with R. M. More, E. Startsev, and I. Kaganovich. This work was performed under the auspices of the U.S. Department of Energy by Lawrence Livermore National Security, LLC, Lawrence Livermore National Laboratory under Grant No. DE-AC52-07NA27344, and by UC Berkeley under Grant No. DE-FG02-04ER41289. This material is based upon work supported by the U.S. D.O.E., Office of Science, Fusion Energy Sciences.

[1] F. Perrot, M. W. C. Dharma-Wardana, and J. Benage, Possibility of an unequivocal test of different models of the equation of state of aluminum in the coupling regime $\Gamma \sim$ 1-50, Phys. Rev. E **65**, 046414 (2002).

[2] R. W. Lee, H. A. Baldis, R. C. Cauble, O. L. Landen, J. S. Wark, A. Ng, S. J. Rose, C. Lewis, D. Riley, J.-C. Gauthier, and P. Audebert, Plasma-based studies with intense x-ray and particle beam sources, Laser Particle Beams **20**, 527 (2002).

[3] M. Koenig, A. Benuzzi-Mounaix, A. Ravasio, T. Vinci, N. Ozaki, S. Lepape, D. Batani, G. Huser, T. Hall, D. Hicks, A. MacKinnon, P. Patel, H. S. Park, T. Boehly, M. Borghesi, S. Kar, and L. Romagnani, Progress in the study of warm dense matter, Plasma Phys. Control. Fusion **47**, B441 (2005).

[4] A. Forsman, A. Ng, G. Chiu, and R. M. More, Interaction of femtosecond laser pulses with ultrathin foils, Phys. Rev. E **58**, R1248 (1998).

[5] D. H. H. Hoffmann, A. Blazevic, O. N. Rosmej, P. Spiller, N. A. Tahir, K. Weyrich, T. Dafni, M. Kuster, M. Roth, S. Udrea, D. Varentsov, J. Jacoby, K. Zioutas, V. Mintsev, V. E. Fortov, B. Y. Sharkov, and Y. Maron, Frontiers of dense plasma physics with intense ion and laser beams and accelerator technology, Physica Scripta **2006**, 1 (2006).

[6] J. J. Barnard, J. Armijo, R. M. More, A. Friedman, I. Kaganovich, B. G. Logan, M. M. Marinak, G. E. Penn, A. B. Sefkow, R. Santhanam, P. Stoltz, S. Veitzer, and J. S. Wurtele, Theory and simulation of warm dense matter targets, Nucl. Instrum. Methods Phys. Res. A **577**, 275 (2007).

[7] F. M. Bieniosek, J. J. Barnard, A. Friedman, E. Henestroza, J. Y. Jung, M. A. Leitner, S. Lidia, B. G. Logan, R. M. More, P. A. Ni, P. K. Roy, P. A. Seidl, and W. L. Waldron, Ion-beam-driven warm dense matter experiments, J. Phys.: Conf. Ser. **244**, 032028 (2010).

[8] N. A. Tahir, D. H. H. Hoffmann, A. Kozyreva, A. Shutov, J. A. Maruhn, U. Neuner, A. Tauschwitz, P. Spiller, and R. Bock, Equation-of-state properties of high-energy-density matter using intense heavy ion beams with an annular focal spot, Phys. Rev. E **62**, 1224 (2000).

[9] M. Koenig, A. Benuzzi, B. Faral, J. Krishnan, J. M. Boudenne, T. Jalinaud, C. Remond, A. Decoster, D. Batani, D. Beretta, and T. A. Hall, Brominated plastic equation of state measurements using laser driven shocks, Appl. Phys. Lett. **72**, 1033 (1998).

[10] A. Rakhel, A. Kloss, and H. Hess, On the critical point of tungsten, Int. J. Thermophys. **23**, 1369 (2002).

[11] G. F. B. Riemann, Ueber die Fortpflanzung ebener Luftwellen von endlicher Schwingungsweite, Abhandlungen der Königlichen Gesellschaft der Wissenschaften in Göttingen **8**, 43 (1860).

[12] Y. B. Zeldovich and Y. P. Raizer, *Physics of Shock Waves and High-Temperature Hydrodynamic Phenomena* (Dover Publications, London, 1962).

[13] L. D. Landau and E. M. Lifshitz, *Fluid Mechanics* (Butterworth-Heinemann, Oxford, UK, 1987).

[14] D. von der Linde, K. Sokolowski-Tinten, and J. Bialkowski, Laser-solid interaction in the femtosecond time regime, Appl. Surf. Sci. **109–110**, 1 (1997).

[15] K. Sokolowski-Tinten, J. Bialkowski, A. Cavalleri, D. von der Linde, A. Oparin, J. Meyer-ter-Vehn, and S. I. Anisimov, Transient states of matter during short pulse laser ablation, Phys. Rev. Lett. **81**, 224 (1998).

[16] N. A. Inogamov, Y. V. Petrov, S. I. Anisimov, A. M. Oparin, N. V. Shaposhnikov, D. von der Linde, and J. Meyer-ter-Vehn, Expansion of matter heated by an ultrashort laser pulse, J. Exp. Theoret. Phys. Lett. **69**, 310 (1999).

[17] V. Zhakhovskii, K. Nishihara, S. Anisimov, and N. Inogamov, Molecular-dynamics simulation of rarefaction waves in media that can undergo phase transitions, J. Exp. Theoret. Phys. Lett. **71**, 167 (2000).

[18] J. J. Barnard, Hydromotion in WDM (Lawrence Berkeley National Laboratory School: Warm Dense Matter School, Berkeley, CA, 10–16 January, 2008).
[19] S. I. Anisimov, N. A. Inogamov, A. M. Oparin, B. Rethfeld, T. Yabe, M. Ogawa, and V. E. Fortov, Pulsed laser evaporation: Equation-of-state effects, Appl. Phys. A: Mater. Sci. Process. **69**, 617 (1999).
[20] M. E. Foord, D. B. Reisman, and P. T. Springer, Determining the equation-of-state isentrope in an isochoric heated plasma, Rev. Sci. Instrum. **75**, 2586 (2004).
[21] N. M. Bulgakova, I. M. Bourakov, and N. A. Bulgakova, Rarefaction shock wave: Formation under short pulse laser ablation of solids, Phys. Rev. E **63**, 046311 (2001).
[22] N. M. Bulgakova and I. M. Burakov, Nonlinear hydrodynamic waves: Effects of the equation of state, Phys. Rev. E **70**, 036303 (2004).
[23] E. Startsev, I. Kaganovich, and R. Davidson, in *Workshop on High Power Lasers, SLAC* (Stanford, October 1–2, 2013).
[24] R. M. More, DISH user manual, LBNL Report (August, 2007).
[25] D. Chandler, J. D. Weeks, and H. C. Andersen, Van der waals picture of liquids, solids, and phase transformations, Science **220**, 787 (1983).
[26] G. Soave, Improvement of the van der Waals equation of state, Chem. Eng. Sci. **39**, 357 (1984).
[27] W. Y. Liu, J. J. Barnard, A. Friedman, N. D. Masters, A. C. Fischer, A. E. Koniges, and D. C. Eder, Modeling droplet breakup effects with diffuse interface methods in ale-amr code with application in modeling NDCX-II experiments, Bull. Am. Phys. Soc. **56**(16), 9.00082 (2011).
[28] T. L. Hill, *An Introduction to Statistical Thermodynamics* (Dover Publications, London, 1987).
[29] D. R. Lide, *Handbook of Chemistry and Physics*, 93rd ed. (CRC Press, Boca Raton, 2012).
[30] C. Kittel, *Elementary Statistical Physics* (Dover Publications, London, 2004).
[31] S. Wolfram, *The MATHEMATICA Book, Version 4* (Cambridge University Press, Cambridge, 1999).